

AD-A089 185

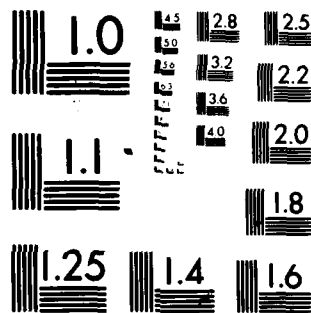
AEROSPACE CORP EL SEGUNDO CA VEHICLE ENGINEERING DIV F/6 16/3  
NOSE TIP SHAPE OPTIMIZATION FOR MINIMUM TRANSPIRATION COOLANT R--ETC(U)  
SEP 80 R L BAKER, R F KRAMER F04701-79-C-0080  
TR-0080(5550-01)-3 SD-TR-80-64 NL

UNCLASSIFIED

1 1 1  
1 1 1

1 1 1


END  
DATE  
FILMED  
10 80  
DTIC



MICROCOPY RESOLUTION TEST CHART  
NATIONAL BUREAU OF STANDARDS-1963-A

**LEVEL II**

AD A089185

# **Nose Tip Shape Optimization for Minimum Transpiration Coolant Requirements**

**R. L. BAKER**  
Vehicle Engineering Division  
and  
**R. F. KRAMER**  
Information Processing Division  
The Aerospace Corporation

15 September 1980

APPROVED FOR PUBLIC RELEASE;  
DISTRIBUTION UNLIMITED

DTIC  
ELECTE  
SEP 15 1980

A

DDC FILE COPY

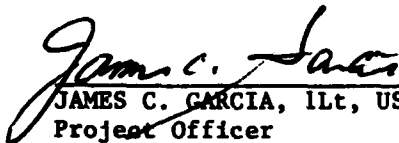
Prepared for  
SPACE DIVISION  
AIR FORCE SYSTEMS COMMAND  
Los Angeles Air Force Station  
P.O. Box 92960, Worldway Postal Center  
Los Angeles, Calif. 90009


80 9 15 029

This final report was submitted by The Aerospace Corporation, El Segundo, CA 90245, under Contract F04701-79-C-0080 with the Space Division, Deputy for Reentry Systems, P.O. Box 92960, Worldway Postal Center, Los Angeles, CA 90009. It was reviewed and approved for The Aerospace Corporation by E.G. Hertler, Principal Director, AeroEngineering Subdivision, Vehicle Engineering Division, and D.H. Landauer, Director, ABRES Liaison Program Office, Engineering Group. The Air Force project officer was 1Lt James C. Garcia, SD/YLXT.

This report has been reviewed by the Public Affairs Office (PAS) and is releasable to the National Technical Information Service (NTIS). At NTIS, it will be available to the general public, including foreign nations.

This technical report has been reviewed and is approved for publication. Publication of this report does not constitute Air Force approval of the report's findings or conclusions. It is published only for the exchange and stimulation of ideas.

  
JAMES C. GARCIA, 1Lt, USAF  
Project Officer

  
JOSEPH J. COX, JR., LtCol, USAF  
Chief, Advanced Technology Division

FOR THE COMMANDER

  
BURTON H. HOLADAY, Col, USAF  
Director of Space Systems Planning  
Deputy for Technology

UNCLASSIFIED

SECURITY CLASSIFICATION OF THIS PAGE (When Data Entered)

19 REPORT DOCUMENTATION PAGE		READ INSTRUCTIONS BEFORE COMPLETING FORM	
1. REPORT NUMBER SD-TR-80-64	2. GOVT ACCESSION NO. AD-A089185	3. RECIPIENT'S CATALOG NUMBER	
4. TITLE (and Subtitle) NOSE TIP SHAPE OPTIMIZATION FOR MINIMUM TRANSPIRATION COOLANT REQUIREMENTS.		5. TYPE OF REPORT & PERIOD COVERED Final Report, : Aug 76-30 Jun 78	
7. AUTHOR(s) R. L. Baker and R. F. Kramer		6. PERFORMING ORG. REPORT NUMBER TR-0080(5550-01)-3	
9. PERFORMING ORGANIZATION NAME AND ADDRESS The Aerospace Corporation ✓ El Segundo, Calif. 90245		8. CONTRACT OR GRANT NUMBER(s) F04701-79-C-0080	
11. CONTROLLING OFFICE NAME AND ADDRESS Space Division Air Force Systems Command Los Angeles, Calif. 90009		10. PROGRAM ELEMENT, PROJECT, TASK AREA & WORK UNIT NUMBERS	
14. MONITORING AGENCY NAME & ADDRESS (if different from Controlling Office) 12 144		12. REPORT DATE 15 Sep 1980	
		13. NUMBER OF PAGES 38	
		15. SECURITY CLASS. (of this report) Unclassified	
		15a. DECLASSIFICATION/DOWNGRADING SCHEDULE	
16. DISTRIBUTION STATEMENT (of this Report)  Approved for public release; distribution unlimited.			
17. DISTRIBUTION STATEMENT (of the abstract entered in Block 20, if different from Report)			
18. SUPPLEMENTARY NOTES			
19. KEY WORDS (Continue on reverse side if necessary and identify by block number)  Nosetip Minimum Heat Transfer Transpiration			
20. ABSTRACT (Continue on reverse side if necessary and identify by block number)  Expressions for the total heat transfer to a nose tip for a realistic reentry trajectory have been obtained by using local laminar and turbulent convective heat transfer relationships and extending the trajectory integration procedures of earlier investigators. Then, employing approximate relationships for the boundary layer edge properties along the nose tip surface, <del>we utilize</del> a variational calculus approach to determine nose tip shapes →			

DD FORM 1473  
(FACSIMILE)

409369

UNCLASSIFIED

SECURITY CLASSIFICATION OF THIS PAGE (When Data Entered)

UNCLASSIFIED

SECURITY CLASSIFICATION OF THIS PAGE(When Data Entered)

19. KEY WORDS (Continued)

IS UTILIZED

20. ABSTRACT (Continued)

which minimize the total trajectory heat transfer (coolant requirements) for fixed fineness ratio and reentry parameters. The calculated minimum heat transfer shapes found have a flat nose with an expansion corner followed by an afterbody with monotonically decreasing slope. The height of the flat nose relative to the base radius decreases as the fineness ratio decreases. However, for fineness ratios greater than 0.2, the laminar and turbulent solution shapes were found to be very similar to one another. For fineness ratios approaching zero (i.e., slender bodies), the laminar and turbulent minimum heat transfer shapes are  $1/2$  and  $8/13$  power law bodies, respectively. The relative heat transfer rate to a particular one of the minimum heat transfer shapes was found to be a factor of up to three times lower than that for other body shapes having the same fineness ratio.

UNCLASSIFIED

SECURITY CLASSIFICATION OF THIS PAGE(When Data Entered)

# PREFACE

The contributions to this work through extended personal communications of Mr. Peter Crowell are gratefully acknowledged.

Accession For	
NRIS General	<input checked="" type="checkbox"/>
DDI TAB	<input type="checkbox"/>
Unprocessed	<input type="checkbox"/>
or collection	
By	
Institution/	
Availability Codes	
Dist	Field and/or special
A	

## CONTENTS

PREFACE . . . . .	1
I. INTRODUCTION . . . . .	5
II. HEAT TRANSFER PREDICTION METHODS . . . . .	7
A. Integrated Heat Transfer Expressions . . . . .	7
B. Evaluation of $I_Q^L$ and $I_Q^T$ . . . . .	10
C. Local Properties on a Flat Face . . . . .	12
III. THE VARIATIONAL PROBLEM . . . . .	15
A. Mathematical Formulation . . . . .	15
B. Interpretation of Solutions . . . . .	17
C. Computation of Solutions . . . . .	19
IV. RESULTS AND DISCUSSION . . . . .	21
A. Minimum Heat Transfer Solutions . . . . .	21
B. Comparison with Other Body Shapes . . . . .	28
C. Solution Characteristics and Accuracy . . . . .	30
V. SUMMARY AND CONCLUSIONS . . . . .	33
APPENDICES:	
A. SLENDER BODY MINIMUM HEAT TRANSFER SHAPES . . . . .	35
B. HEAT TRANSFER INTEGRALS--SLENDER BODY THEORY . . . . .	37
C. STABLE ABLATING NOSETIP SHAPES . . . . .	39



## FIGURES

1.	Nose Tip Geometry and Coordinate System . . . . .	11
2.	Minimum Laminar Heat Transfer Shapes . . . . .	22
3.	Minimum Laminar and Turbulent Heat Transfer Shapes . . .	24
4.	Minimum $I_Q$ as a Function of Fineness Ratio . . . . .	25
5.	Body Shape Comparisons . . . . .	26
6.	Minimum and Maximum $I_Q$ Values Compared with Other Body Shapes . . . . .	27
7.	Flat-Face Height versus Fineness Ratio . . . . .	32

## TABLE

1.	Body Angle Aft of Expansion Corner for Different Variational Calculus Solutions . . . . .	31
----	----------------------------------------------------------------------------------------------	----

## I. INTRODUCTION

For some applications, a decrease in the amount of coolant required for a transpiration-cooled reentry vehicle nose tip is desirable and potentially very beneficial. The work presented here seeks to optimize the shape of a reentry vehicle nose tip in order to minimize the total heat transferred (and thus the transpiration coolant requirements) to the nose tip throughout a realistic reentry trajectory. The nose tip shape is assumed to remain constant throughout the trajectory.

The majority of work devoted to the determination of optimum body shapes in a hypersonic flow environment has been concerned with the problem of finding minimum drag bodies<sup>1</sup>. Recently, however, work has appeared which considers the determination of minimum heat transfer body shapes in a constant freestream environment. Laminar flow solutions were found by Belyanin<sup>2</sup> and Aihara<sup>3</sup>. Belyanin discussed the relative heat flux to his minimum heat transfer solution bodies, but did not give any details of the body shapes. Aihara's solution has been shown by Hull<sup>4</sup> not to be a minimum solution. Perminov and Solodkin<sup>5</sup> obtained nonslender body solutions for both minimum total drag and minimum heat transfer for both laminar and

<sup>1</sup>Miele, A. (ed.), "Theory of Optimum Aerodynamic Shapes," Applied Mathematics and Mechanics, 9, Academic Press, New York (1965).

<sup>2</sup>Belyanin, N.M., "Determining the Form of a Body Resulting in Minimum Heat Flux, with Laminar Flow in the Boundary Layer," Izv, AN SSSR, Mekhanika Zhidkosti i Gaza, 2(6), pp. 37-45 (1967). English Translation, Fluid Dynamics, Consultant's Bureau, New York (1969).

<sup>3</sup>Aihara, Y., "Optimum Body Geometries of Minimum Heat Transfer at Hypersonic Speeds," AIAA Journal, Technical Notes, 6(11), pp. 2187-2188 (November 1968).

<sup>4</sup>Hull, D.G., "On Hypersonic Shapes of Minimum Heat Transfer," The Journal of the Astronautical Sciences, XVII(1), pp. 60-62 (July-August 1969).

<sup>5</sup>Perminov, V.D., and E.E. Solodkin, "Axisymmetrical Bodies with Minimal Resistance and with Minimal Flow Toward the Surface of the Body, with Different Characters of the Flow in the Boundary Layer," Izvestiya Akademii Nauk SSSR, Mekhanika Zhidkosti i Gaza, (2), pp. 94-102 (March-April 1971). English Translation, Fluid Dynamics, Consultant's Bureau, New York (1973).

turbulent flow. They found the laminar and turbulent minimum heat transfer shapes to be very similar to one another for a given fineness ratio. The work presented here extends this previous work to the case of a reentry trajectory environment and seeks to minimize the total heat transfer to the nose tip for the entire trajectory.

Section II first presents a brief derivation of the total heat transfer relationships used in this work and the approximate flow field evaluation procedures utilized. Then, in Section III, the mathematical formulation of the minimum heat transfer problem using a variational calculus approach is discussed. Calculated results are then given which discuss both minimum and maximum heat transfer solutions and the relative heat transfer rates to these shapes compared with several other body shapes.

## II. HEAT TRANSFER PREDICTION METHODS

### A. INTEGRATED HEAT TRANSFER EXPRESSIONS

When expressions for the laminar and turbulent convective heat transfer coefficient given by Vaglio-Laurin<sup>6, 7</sup> are used, and the procedure of Allen and Eggers<sup>8</sup> is followed, the rate of change of integrated heat transfer with altitude  $dQ/dy$  is given by

$$\frac{dQ}{dy} = \frac{C_n \rho_\infty V_\infty^2 \pi r_B^2}{Re_o^{n/n+1} \sin \theta_E} \int_0^{\bar{s}} \frac{\bar{\rho}_e \bar{u}_e \bar{\mu}_e \bar{r}^{n+1} d\bar{s}}{\left[ \int_0^{\bar{s}} \bar{\rho}_e \bar{u}_e \bar{\mu}_e \bar{r}^{n+1} d\bar{s} \right]^{n/n+1}} \quad (1)$$

where  $n = 1$  for laminar flow and  $n = 1/4$  for turbulent flow. When the integration in nondimensional surface distance  $\bar{s} = s/r_B$  is performed, this expression becomes

$$\frac{dQ}{dy} = \frac{-(n+1) C_n \rho_\infty V_\infty^2 \pi r_B^2}{Re_o^{n/n+1} \sin \theta_E} I_Q^{1/n+1} \quad (2)$$

where the integral  $I_Q$  is given by

$$I_Q = \int_0^{\bar{s}} \bar{\rho}_e \bar{u}_e \bar{\mu}_e \bar{r}^{n+1} d\bar{s} \quad (3)$$

<sup>6</sup> Vaglio-Laurin, R., "Laminar Heat Transfer on Three-Dimensional Blunt Nosed Bodies in Hypersonic Flow," ARS Journal, 29(2), pp. 123-129 (February 1959).

<sup>7</sup> Vaglio-Laurin, R., "Turbulent Heat Transfer on Blunt Nosed Bodies in Two-Dimensional and General Three-Dimensional Hypersonic Flow," Journal of the Aero/Space Sciences, 27(1), pp. 27-36 (January 1960).

<sup>8</sup> Allen, H. Julian, and A.J. Eggers, Jr., "A Study of the Motion and Aerodynamic Heating of Ballistic Missiles Entering the Earth's Atmosphere at High Supersonic Speeds," NACA Report 1381 (1958).

Allen and Eggers integrated an expression analogous to Eq. (2), representing  $\rho_\infty$  and  $V_\infty$  as functions of altitude  $y$  from their trajectory analysis and assuming  $Re_0$  to be constant. In the present analysis, the shock layer Reynolds number  $Re_0$  is represented as a function of  $y$ . Then, following the general integration procedure of Brunner<sup>9</sup>, the total integrated heat transfer to a body throughout a trajectory is given for laminar flow by

$$Q^L = C_{fE}^L r_B^{3/2} [\beta_{IQ}^L]^{1/2} \operatorname{erf} \left( \sqrt{B^L} \right) \quad (4)$$

and for turbulent flow by

$$Q^T = C_{fE}^T r_B^{9/5} [\beta_{IQ}^T]^{4/5} \int_0^{[B^T]^{4/5}} e^{-t^{5/4}} dt \quad (5)$$

The complete derivation of Eqs. (4) and (5) is given in Ref. 10. The  $\beta$  and  $r_B$  in these equations are the ballistic coefficient and the base radius, respectively. In the derivation of these equations, the ballistic coefficient has been assumed to be constant throughout the trajectory. This is a reasonably good assumption over the altitude range of importance for convective heat transfer, i. e., less than 100 kft. Optimum shapes allowing for the changes in  $\beta$  through a trajectory have been reported recently.<sup>11</sup> The

<sup>9</sup>Brunner, M. J., "Analysis of Aerodynamic Heating for a Re-entrant Space Vehicle," Journal of Heat Transfer, 81(8), pp. 223-229 (August 1959).

<sup>10</sup>Baker, R. L., and R. F. Kramer, "Evaluation of Total Heat Transfer in Hypersonic Flow Environments," Report No. TR-0077(2550-15)-6, The Aerospace Corporation, El Segundo, California.

<sup>11</sup>Yelmgren, Capt. Kevin E., "Optimum Nose Shape for Transpiration-Cooled Reentry Vehicles," AFFDL TR-78-1117, Air Force Flight Dynamics Laboratory (November 1978).

other parameters are given by

$$C^L = 1.866 \times 10^{-6} \left[ \frac{\left( \frac{\gamma+1}{\gamma-1} \right)}{(2\omega+3)\lambda} \right]^{1/2}, \quad C^T = \frac{4.70 \times 10^{-6}}{\lambda^{1/5}} \left[ \frac{\left( \frac{\gamma+1}{\gamma-1} \right)}{(2\omega+9)} \right]^{4/5} \quad (6a, b)$$

$$f_E^L = \frac{\mu_E^{1/2} V_E^{3/2}}{(\sin \theta_E)^{1/2}}, \quad f_E^T = \frac{\mu_E^{1/5} V_E^{9/5}}{(\sin \theta_E)^{1/5}} \quad (7a, b)$$

$$I_Q^L = \int_0^{\bar{s}} \bar{\rho}_e \bar{u}_e \bar{\mu}_e \bar{r}^2 d\bar{s}, \quad I_Q^T = \int_0^{\bar{s}} \bar{\rho}_e \bar{u}_e \bar{\mu}_e \bar{r}^{5/4} d\bar{s} \quad (8a, b)$$

$$B = \left[ \frac{\rho^0}{\lambda \beta \sin \theta_E} \right], \quad B^L = \frac{(2\omega+3)}{4} B, \quad B^T = \frac{(2\omega+9)}{10} B \quad (9a, b, c)$$

The variables in these equations are the air specific heat ratio and viscosity law exponent,  $\gamma$  and  $\omega$ ; the density scale height factor in the exponential atmosphere,  $\lambda$ ; the reentry velocity and entry flight path angle,  $V_E$  and  $\theta_E$ ; the air viscosity evaluated at the entry stagnation temperature,  $\mu_E$ ; the ballistic factor  $B$  and the heat transfer integrals  $I_Q^L$  and  $I_Q^T$  which depend upon an integration in body surface running length of the local boundary layer edge density,  $\bar{\rho}_e$ , velocity  $\bar{u}_e$ , viscosity,  $\bar{\mu}_e$ , and local radial coordinate  $\bar{r}$ .

As indicated earlier, previous investigators have sought to minimize the integrated heat transfer to a body for the case in which the freestream environment is constant. Using the Vaglio-Laurin convective heat transfer relationships and integrating over the surface area as in Eq. (1) results in

the following expression for the integrated heat transfer rate to a body in a constant environment for laminar flow<sup>10</sup>

$$\frac{dQ^L/dt}{\rho_{\infty} V_{\infty} H_o (\pi r_B^2)} = 1.328 \left( \frac{\gamma+1}{\gamma-1} \right) \left[ I_Q^L \right]^{1/2} Re_o^{-1/2} \quad (10a)$$

and for turbulent flow

$$\frac{dQ^T/dt}{\rho_{\infty} V_{\infty} H_o (\pi r_B^2)} = 0.0720 \left( \frac{\gamma+1}{\gamma-1} \right) \left[ I_Q^T \right]^{4/5} Re_o^{-1/5} \quad (10b)$$

where  $Re_o$  is a shock layer Reynolds number defined by

$$Re_o = \frac{\rho_o (2H_o)^{1/2} r_B}{\mu_o} \quad (11)$$

It is now evident that if we fix  $f_E^L$ ,  $r_B$ ,  $\beta$  and  $B^L$  in Eq. (4) or  $\rho_{\infty} V_{\infty}$ ,  $H_o$ ,  $r_B$  and  $Re_o$  in Eq. (10a), then the total heat transfer  $Q^L$  in the first case and the total heat transfer rate  $dQ^L/dt$  in the second case will be minimized if we minimize the integral  $I_Q^L$ . Similarly, in the turbulent case  $Q^T$  and  $dQ^T/dt$  are minimized by minimizing the integral  $I_Q^T$ . The relationship of the ballistic trajectory environment problem considered in this work to the constant environment problem considered by other investigators is thus established.

#### B. EVALUATION OF $I_Q^L$ and $I_Q^T$

The heat transfer integrals  $I_Q^L$  and  $I_Q^T$ , given by Eqs. (8a) and (8b), respectively, depend intimately upon the nose tip geometry, i. e., upon the shape contour of the nose tip. As shown in Fig. 1, the local nose tip coordinates  $r$  and  $z$  and the surface running length  $s$  are related to the local nose tip surface angle  $\alpha$  by the following simple trigonometric relationships

$$\frac{dr}{dz} = \tan \alpha, \quad \frac{ds}{ds} = \sin \alpha \quad (12)$$

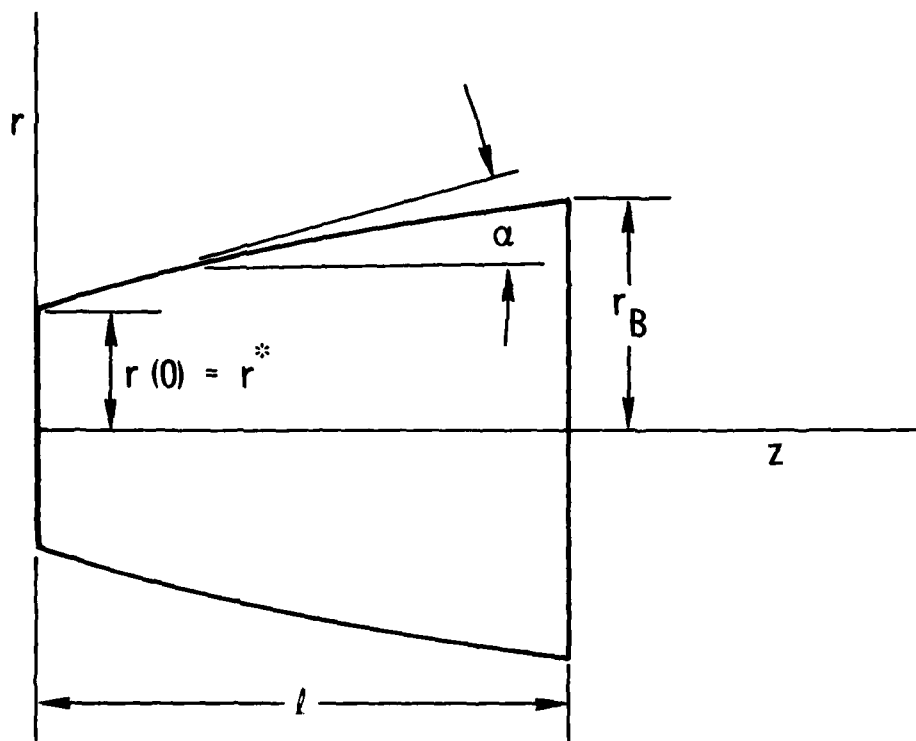


Fig. 1. Nose Tip Geometry and Coordinate System



To a reasonably good approximation the local nondimensional boundary layer edge properties  $\bar{\rho}_e$ ,  $\bar{u}_e$  and  $\bar{\mu}_e$  in Eqs. (8a) and (8b) may be represented as functions of  $\alpha$ . In the present work the simplest equations of this type have been used, i. e., the hypersonic Newtonian approximations for both pressure and velocity. Thus, the local pressure  $\bar{p}_e = p_e/p_{t_2}$  is given by

$$\bar{p}_e = \sin^2 \alpha \quad (13)$$

and the local velocity  $\bar{u}_e = u_e/\sqrt{2H_0}$  is given by

$$\bar{u}_e = \cos \alpha \quad (14)$$

If the viscosity is assumed to be proportional to the temperature and independent of pressure, the density-viscosity product is then directly proportional to the pressure, i. e.

$$\bar{\rho}_e \bar{\mu}_e = \frac{\rho_e \mu_e}{\rho_0 \mu_0} = \sin^2 \alpha \quad (15)$$

The utility rendered by the simplicity of these equations was felt to compensate for inherent inaccuracies associated with them for purposes of comparing relative heat transfer rates to various nose tip shapes as discussed herein. Work is currently in progress to reconsider the problem discussed in this report and to replace the approximations given by Eqs. (13) through (15) with numerical inviscid flow field calculation procedures. Numerical flow field calculations for fixed body shapes somewhat similar to those discussed here, i. e., flat-face cones, are given in Ref. 10.

### C. LOCAL PROPERTIES ON A FLAT FACE

In order to allow for solutions which may have a flat face, it is necessary to have an alternate expression for the boundary layer edge velocity  $\bar{u}_e$ . This is because direct use of Eq. (14) would indicate that  $\bar{u}_e$  and, therefore,  $I_Q^L$  and  $I_Q^T$  are all identically zero on a flat face. In Refs. 2 and 5, the following approximation for the  $\rho_e u_e \mu_e$  product, obtained from a correlation of method of integral relations solutions, was used.

$$\frac{\rho_e u_e \mu_e}{[\rho_e u_e \mu_e]^*} = \frac{\bar{r}}{\bar{r}^*} \quad (16)$$

Equation (16) indicates that for a flat-faced body, the normalized  $\rho_e u_e \mu_e$  product varies linearly with distance to the sonic point. The sonic point values of the dependent variables may be obtained by isentropic expansion from the stagnation conditions. The terms  $\rho_e$ ,  $u_e$  and  $\mu_e$  in Eq. (16) may then be renormalized by the stagnation values  $\rho_o$ ,  $\sqrt{2H_o}$ ,  $\mu_o$ . Using ideal gas relationships, we obtain

$$\bar{\rho}_e \bar{u}_e \bar{\mu}_e = \frac{\rho_e u_e \mu_e}{\rho_o (2H_o)^{1/2} \mu_o} = F(\gamma) \frac{\bar{r}}{\bar{r}^*} \quad (17a)$$

$$F(\gamma) = \left[ \frac{\gamma+1}{2} \right]^{\gamma/1-\gamma} \left[ \frac{\gamma-1}{\gamma+1} \right]^{1/2} \quad (17b)$$

In Section III, Eqs. (12) through (17) are used to express the heat transfer integral  $I_Q$  explicitly in terms of the body geometry.

### III. THE VARIATIONAL PROBLEM

#### A. MATHEMATICAL FORMULATION

This section will be concerned with the determination of those shapes which in a limited sense produce extreme values of  $I_Q$ . Body shapes with a flat forward face of height  $r^*$ , possibly zero, will be considered (see Fig. 1).

Normalizing all coordinates by  $r_B$ , define

$$x = z/r_B, \quad y = r/r_B \quad (18)$$

The Newtonian flow approximations, Eqs. (14) and (15), and the geometric relationships, Eqs. (12), may be substituted into the expressions for  $I_Q$ , Eqs. (8a) and (8b), to produce the following expression for  $I_Q$  along the body:

$$[I_Q]_{\text{body}} = \int_0^{2/\tau} \frac{y^{n+1.2}}{1 + \dot{y}^2} dx, \quad \cdot = \frac{d}{dx} \quad (19)$$

Similarly, integrating Eq. (8), using approximation (17a), over a flat face yields

$$[I_Q]_{\text{face}} = \frac{F(\gamma)}{n+3} [y(0)]^{n+2} \quad (20)$$

Thus, the total value of  $I_Q$  may be expressed as

$$I_Q = \frac{F(\gamma)}{n+3} [y(0)]^{n+2} + \int_0^{2/\tau} \frac{y^{n+1.2}}{1 + \dot{y}^2} dx \quad (21)$$

Since  $\tau$  is defined to be the ratio of the diameter to the length of the body,

$$y(2/\tau) = 1 \quad (22)$$

We wish to determine the function  $y(x)$ , chosen from a suitable class of functions on the interval  $0 \leq x \leq 2/\tau$  which minimizes (or maximizes) the functional  $I_Q$ , Eq. (21), and which satisfies the condition (22). Any such minimum (or maximum) must satisfy the Euler equation associated with this problem.

$$\ddot{y} y [1 - 3\dot{y}^2] = - \frac{(n+1)}{2} \dot{y}^2 [1 - \dot{y}^4] \quad (23)$$

The boundary condition  $y(2/\tau) = 1$  is given, but  $y(0)$  is not specified. Hence, this is a variable end point problem of the calculus of variations, and the following transversality condition must be satisfied at  $x = 0$ .

$$y^{n+1} \left[ \frac{\dot{y}}{(1+\dot{y}^2)^2} - \frac{n+2}{2(n+3)} F(y) \right] = 0 \quad (24a)$$

Since the integrand of Eq. (21) is not explicitly a function of  $x$ , a first integral of the Euler equation (23) can be derived. This equation may be written in the following form:

$$y^{n+1} = \frac{C(1+\dot{y}^2)^2}{\dot{y}^2(\dot{y}^2-1)} \quad (24b)$$

Examination of this equation reveals that there is no real value of  $\dot{y}$  which allows  $y$  to be zero. Hence, there is no solution of the Euler equation for which  $y(0) = 0$ .

If a flat-faced,  $y(0) \neq 0$ , solution exists, then [from Eq. (24a)] the initial slope must be a solution of the equation

$$\frac{\dot{y}(0)}{[1 + \dot{y}(0)^2]^2} = \frac{(n+2)}{2(n+3)} F(\gamma) \quad (25)$$

This equation is a quartic in  $\dot{y}(0)$ . An examination of this quartic for the range of parameters  $(n, \gamma)$  of interest reveals two real positive roots and a pair of complex conjugate roots. Thus, there are apparently two functions  $y(x)$  which satisfy the Euler equation and the transversality condition. It should be observed that the values of the two permissible initial slopes are independent of  $\tau$ .

One might expect that the two solutions for  $y(x)$  discussed in the preceding paragraph represent a minimum and a maximum of  $I_Q$ . There are further checks which may be made to verify or limit this conclusion. The necessary condition of Legendre implies that one of the two solutions for  $y(x)$  is a minimum (maximum) if  $\dot{y}(x) \leq \sqrt{3}/3$  [ $\dot{y}(x) \geq \sqrt{3}/3$ ] for all  $x$  in the interval  $0 \leq x \leq 2/\tau$ . The Jacobi condition is somewhat difficult to apply. However, it can be shown that the necessary condition of Weierstrass cannot be satisfied over the class of all possible shapes. Hence, neither of the above solutions corresponds to a minimum or a maximum of  $I_Q$  over the class of all piecewise continuously differentiable functions on the interval  $0 \leq x \leq 2/\tau$  which satisfy the boundary condition Eq. (22). Hull<sup>4</sup> has pointed out a similar occurrence in a related problem.

## B. INTERPRETATION OF SOLUTIONS

The solutions discussed in the preceding subsection are insufficient as global extrema. This may be demonstrated as follows: The integral appearing in Eq. (19) is zero over any segment for which  $\dot{y}$  is zero or for which  $\dot{y}$  is infinite. Hence as  $y(0)$  approaches zero, there are infinite numbers of shapes for which  $I_Q$  is arbitrarily close to zero, i.e., shapes composed of vertical

and horizontal segments. Further consider functions  $y(x)$  which are straight lines between  $y(0)$  at  $x = 0$  and 1 at  $x = 2/\tau$ . As  $y(0)$  becomes arbitrarily large,  $I_Q$  will become arbitrarily large.

The two solutions which satisfy the Euler equation [Eq. (23)], the transversality condition [Eq. (25)] and the boundary condition [Eq. (22)] will be referred to as a "minimum" solution or a "maximum" solution provided they satisfy the Legendre condition for a maximum or a minimum. As has been shown, these solutions do not represent minima or maxima over all possible shapes. However, a minimum solution ( $\dot{y} \leq \sqrt{3}/3$ ) will satisfy the Weierstrass condition for a minimum over the class of all piecewise continuously differentiable functions  $y(x)$  on the interval  $0 \leq x \leq 2/\tau$  for which  $y(2/\tau) = 1$  and for which  $\dot{y}(x) \leq \sqrt{3}/3$  for all  $x$  in the interval. Similarly, a maximum solution ( $\dot{y} \geq \sqrt{3}/3$ ) will satisfy the Weierstrass condition for a maximum over the class of all piecewise continuously differentiable functions  $y(x)$  on the interval  $0 \leq x \leq 2/\tau$  for which  $y(2/\tau) = 1$  and for which  $\dot{y}(x) \geq \sqrt{3}/3$  for all  $x$  in the interval. With these restrictions on derivatives, not only is the Weierstrass condition satisfied, but the Weierstrass-Erdmann corner condition cannot be satisfied by any pair of admissible slopes. Hence, there are no minimum or maximum solutions with discontinuous derivatives.

These limits seemed unduly restrictive. However, after obtaining the solutions it was found that they could be extended. For instance, it was observed that the calculated maximum solutions had the property that  $\dot{y}(x) \geq 1$  for all  $x$ . Examination of the Weierstrass excess function for this problem leads to the following conclusion: If a maximum solution is found whose derivative is greater than or equal to one for all  $x$ , then the  $I_Q$  corresponding to this solution will be larger than the  $I_Q$  corresponding to any piecewise continuously differentiable function  $y(x)$  on the interval  $0 \leq x \leq 2/\tau$  for which  $y(2/\tau) = 1$  and for which  $\dot{y}(x) \geq 0$  for all  $x$  in the interval.

When a minimum solution is found, its maximum derivative  $\dot{y}_{\max}$  over the interval  $0 \leq x \leq 2/\tau$  may be determined. If the constant A is defined by

$$A = \frac{1 - \dot{y}_{\max}^2}{2\dot{y}_{\max}} \quad (26)$$

then examination of the Weierstrass E-function for the problem leads to the following situation. If a minimum solution is found with maximum derivative  $\dot{y}_{\max}$  and constant A, then the  $I_Q$  corresponding to this solution will be smaller than the  $I_Q$  corresponding to any piecewise continuously differentiable function  $y(x)$  on the interval  $0 \leq x \leq 2/\tau$  for which  $y(2/\tau) = 1$  and for which  $\dot{y}(x) \leq A$  for all  $x$  in the interval. It is in this limited sense that the solutions given in the following sections may be considered minima and maxima.

### C. COMPUTATION OF SOLUTIONS

The actual computation of a solution consists of solving a two-point boundary value problem for a second-order nonlinear ordinary differential equation. The differential equation is the Euler equation (23). The boundary conditions are  $y(2/\tau) = 1$  and at  $x = 0$  the transversality condition (25). A program was written to solve a class of such problems, including the one discussed herein. In this program the differential equations and boundary conditions were replaced by finite difference approximations, and the resulting equations were solved by Newton's method (quasilinearization).

#### IV. RESULTS AND DISCUSSION

Results obtained by numerical solution of the Euler equation with appropriate boundary conditions, as discussed above, are presented here for the cases of both laminar and turbulent flow in the boundary layer, i.e.,  $n = 1$  and  $n = 1/4$ , respectively. In all cases the specific heat ratio  $\gamma$  has been assumed to be the hypersonic value of 1.2. In the first subsection below, the body shapes and minimum heat transfer integrals  $I_Q^L$  and  $I_Q^T$  are shown for a wide range of the fineness ratio  $\tau$ . Then, in the next subsection, the minimum heat transfer results are compared with heat transfer rates to other selected body shapes and to some maximum heat transfer solutions.

##### A. MINIMUM HEAT TRANSFER SOLUTIONS

Laminar flow minimum heat transfer shapes for several values of the fineness ratio  $\tau$  are shown in Fig. 2 where the shapes as they appear physically are shown in the upper part of the figure. In the lower part of the figure, the shapes are shown with the radial coordinate normalized by the base radius and the axial coordinate normalized by the body length. In this way the maximum value of both  $\bar{r} = r/r_B$  and  $\bar{z} = z/l$  is unity since two reference lengths have been used. In the remainder of this report, all body shapes will be presented normalized as in the lower part of Fig. 2. It should be kept in mind that presenting results in this way masks the needlelike appearance of shapes with very small fineness ratios  $\tau$  as well as the blunt disklike appearance of shapes with large fineness ratios.

All of the shapes in Fig. 2, for nonzero values of  $\tau$ , exhibit a flat face. The ratio of the radius of the flat face to that of the base increases with increasing  $\tau$ . In the limit of  $\tau$  approaching infinity, the shape becomes a flat-faced cylinder of zero length, i.e., a disk. In the opposite limit, as  $\tau$  approaches zero, the flat-face height approaches zero, and the shape approaches the shape obtained invoking the slender body approximation, i.e., a  $1/2$  power law body<sup>4</sup>. However, since the slender body power law shape is



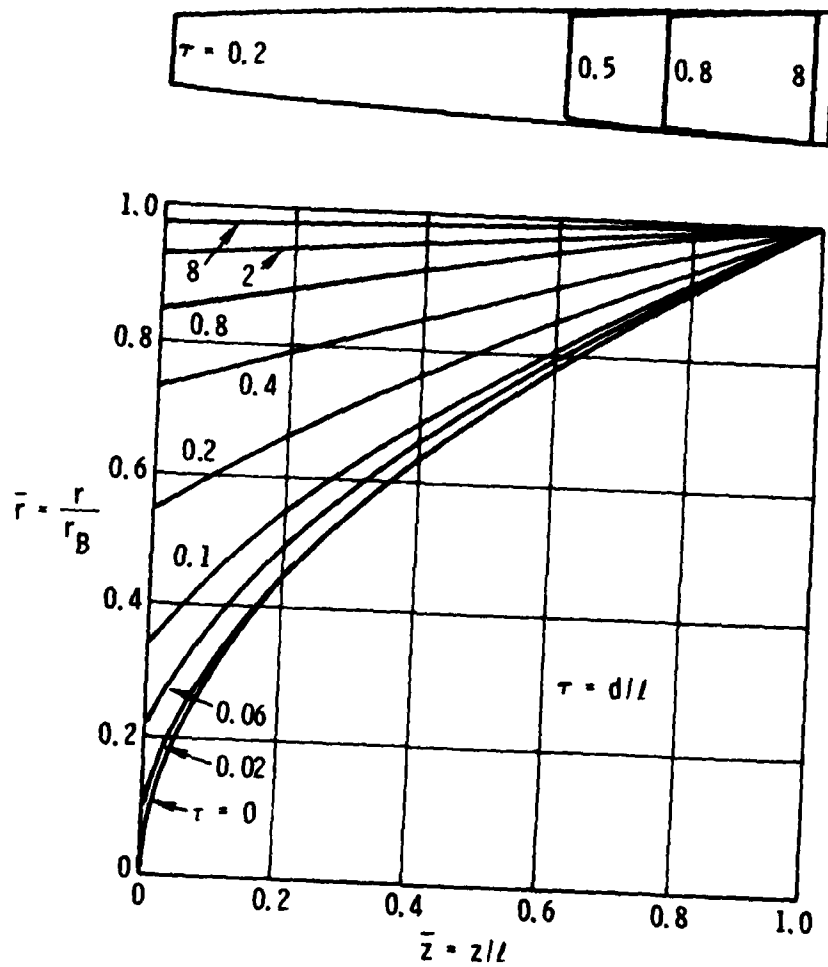


Fig. 2. Minimum Laminar Heat Transfer Shapes

only approached for fineness ratios less than 0.02, this shape appears to be of little practical interest.

In Fig. 3, turbulent flow minimum heat transfer shapes are shown and compared with the laminar shapes for corresponding fineness ratios. As concluded by others<sup>5</sup>, the turbulent shapes are surprisingly similar to the laminar shapes for a given fineness ratio. In the limit of large  $\tau$ , the turbulent minimum heat transfer shape also approaches a flat-faced cylinder; in the limit of  $\tau$  approaching zero it can be easily shown that the turbulent minimum heat transfer shape is an 8/13 power law body. The slender body derivation of power law shapes for minimum laminar and turbulent heat transfer is given in Appendix A. Thus, in the slender body limit the minimum laminar heat transfer shape is a 1/2 power law body, the minimum turbulent heat transfer shape is an 8/13 power law body, and (from Ref. 12) the minimum drag shape is a 3/4 power law body. The non-slender body minimum heat transfer shapes found in the present work approach the slender body minimum heat transfer shapes only at very small fineness ratios ( $\tau < 0.02$ ). However, the nonslender body minimum drag shapes approach a 3/4 power law body at much larger fineness ratios<sup>12</sup> ( $\tau \approx 0.2$ ).

The question of how much reduction in the heat transfer is achieved by a minimum heat transfer shape is considered in the results presented in Figs. 4 through 6 and in the following subsections. Recall that Eqs. (4) and (5) represent expressions for the integrated heat transfer to a nose tip throughout a trajectory. Likewise, Eqs. (10a) and (10b) represent similar expressions for the constant freestream environment case. For all cases, trajectory environment or constant freestream environment, the parameter needed to obtain numerical predictions of heat transfer is the heat transfer integral or body shape parameter  $I_Q$ .

---

<sup>12</sup>Eggers, A.J., Jr., M.M. Resnikoff and D.H. Dennis, "Bodies of Revolution Having Minimum Drag at High Supersonic Speeds," NACA Report No. 1306 (1957).

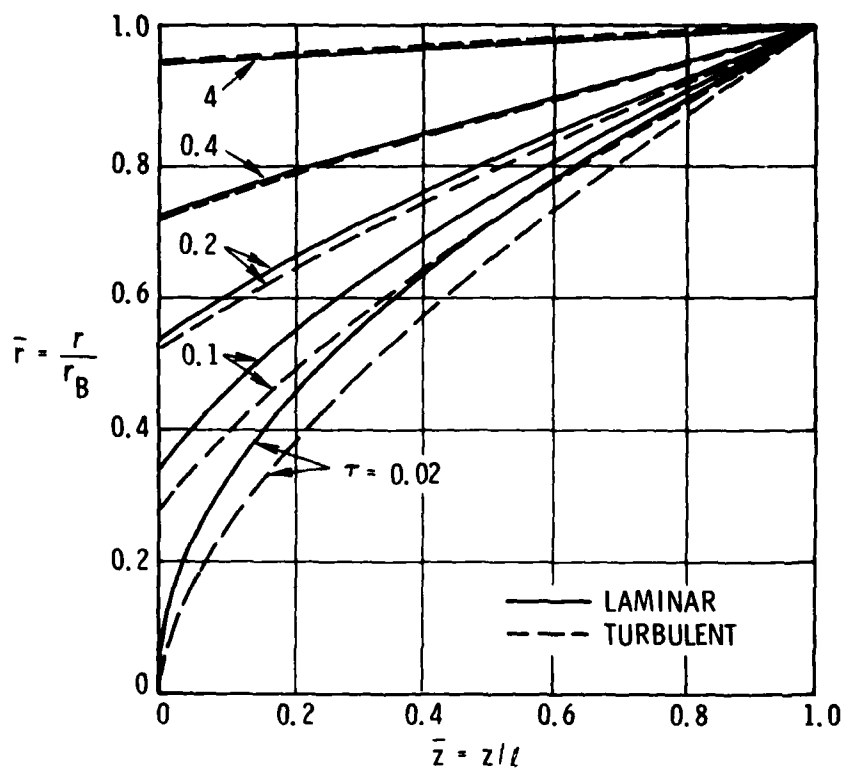


Fig. 3. Minimum Laminar and Turbulent Heat Transfer Shapes

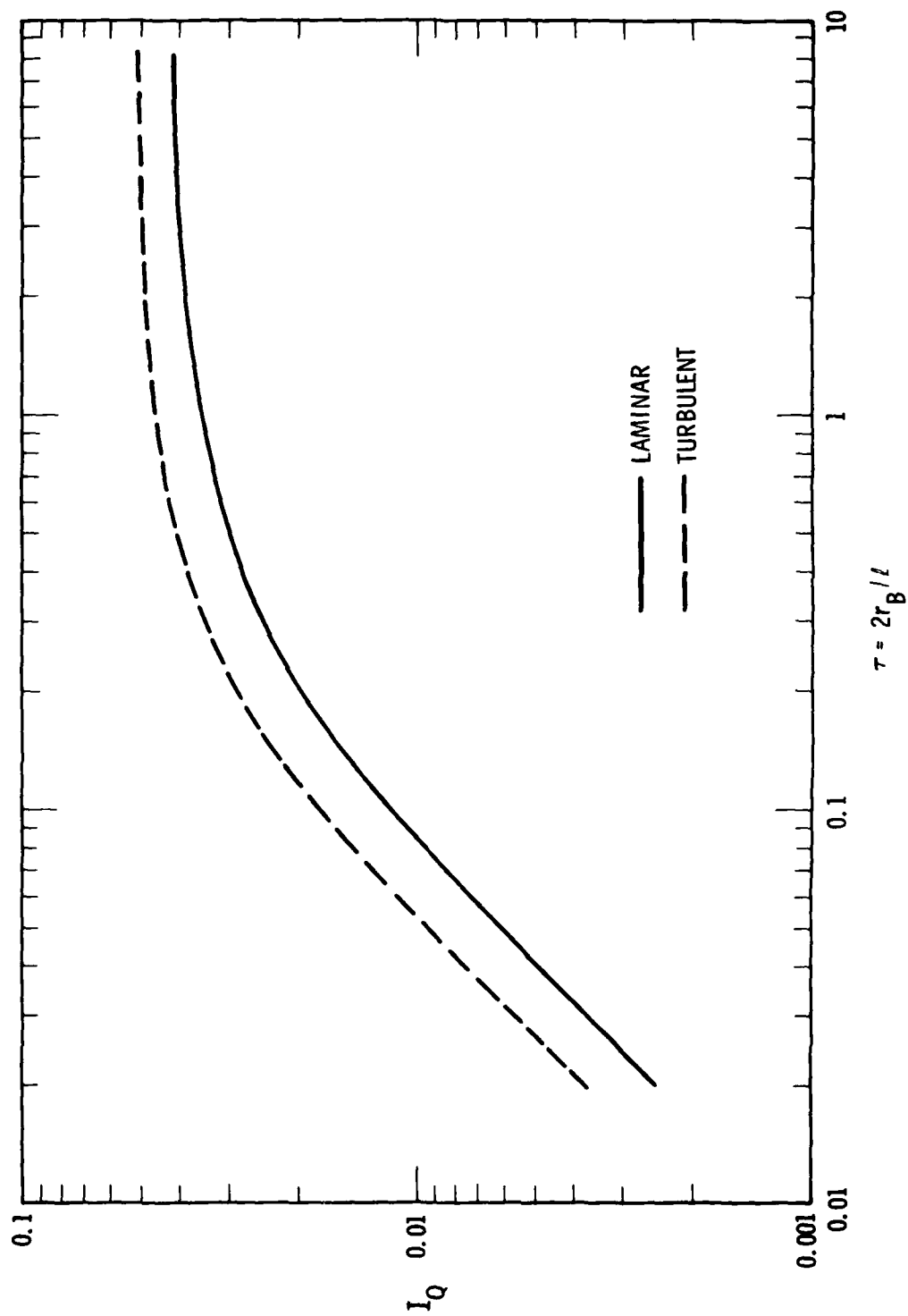


Fig. 4. Minimum  $I_Q$  as a Function of Fineness Ratio

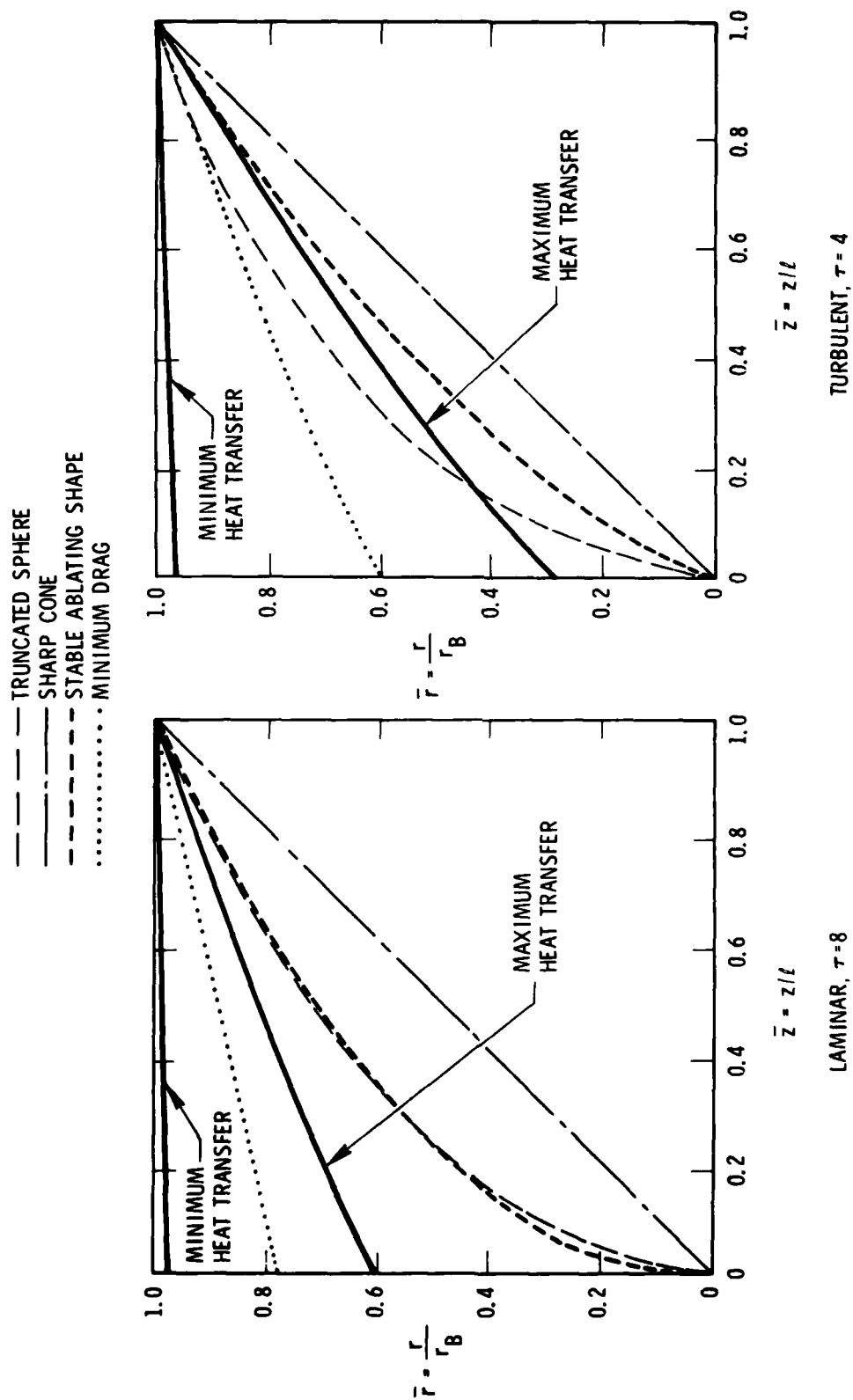


Fig. 5. Body Shape Comparisons

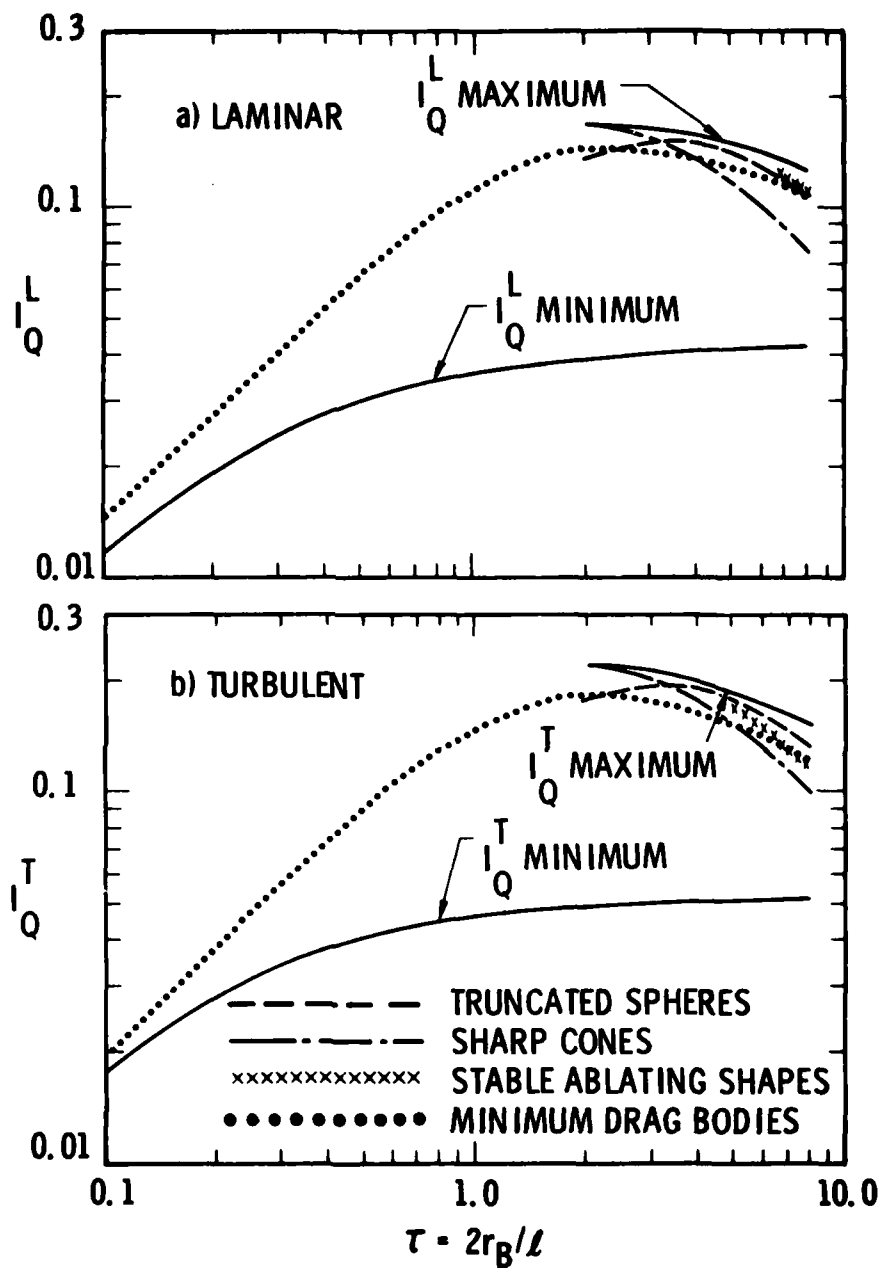


Fig. 6. Minimum and Maximum  $I_Q$  Values Compared with Other Body Shapes

In Fig. 4,  $I_Q$  for the minimum laminar and turbulent heat transfer shapes is shown as a function of  $\tau$ . The  $I_Q$  for both laminar and turbulent flow is quite insensitive to fineness ratio for  $1 < \tau < 10$ . This is because the ratio of flat-face height to base radius is greater than 0.9 for all  $\tau > 1$ . Thus, for  $\tau > 1$ , a large fraction of the total heat transfer occurs over the flat face. However, for  $\tau < 1$  the  $I_Q^L$  and  $I_Q^T$  values decrease significantly as the body or nose tip becomes more slender, i.e., decreasing  $\tau$ . This decrease is due in large part to a significant reduction in the flat-face height, which decreases the area associated with the relatively high flat-face heat transfer.

In the limit of  $\tau$  approaching zero,  $I_Q^L$  and  $I_Q^T$  both go to zero. However,  $I_Q^L/\tau$  and  $I_Q^T/\tau$  are finite for  $\tau = 0$ , and the limiting values are given by slender body theory (see Appendix B). They are

$$\frac{I_Q^L}{\tau} = \frac{1}{8}, \quad \frac{I_Q^T}{\tau} = \frac{32}{169} \quad (27a, b)$$

Comparing the numerical values of  $I_Q^L$  and  $I_Q^T$  from these equations with the nonslender body calculated values in Fig. 4, we see that for  $\tau \leq 0.02$  the slender and nonslender body calculated values are virtually identical. A quantitative comparison of minimum heat transfer rates to those for other body shapes is given below.

#### B. COMPARISON WITH OTHER BODY SHAPES

The minimum heat transfer body shapes and heat transfer integrals discussed above will now be compared with these quantities for a sphere, truncated spheres, sharp cones, minimum drag bodies, stable ablating shapes and maximum heat transfer bodies. Except for the spheres, sharp cones and minimum drag bodies, the remaining body shapes listed above depend upon the boundary layer state, i.e., laminar or turbulent.

The minimum and maximum heat transfer solutions were obtained directly by numerical solution of the Euler equation as discussed previously. The minimum drag body solutions were obtained by application of the present numerical calculation procedure to the appropriate equations as given in Ref. 12. A stable ablating shape is one for which, even though it is ablating and its surface is receding, the body shape contour is independent of time<sup>13</sup>. The following analytic equations for laminar and turbulent stable ablating nose tip shapes, using the approximations given by Eqs. (13) through (15), are derived in Appendix C. For laminar flow

$$\frac{2}{\tau} \bar{z} = \ln \left[ \frac{1 - \sqrt{1 - \bar{r}^2}}{2} \right] - \sqrt{1 - \bar{r}^2} + 1 \quad (28a)$$

and for turbulent flow

$$\frac{2}{\tau} \bar{z} = \frac{4}{3} \bar{r}^{3/4} + \left\{ \frac{1}{2} \left[ \bar{r}^{1/4} \sqrt{1 - \bar{r}^{1/2}} - \sin^{-1}(\bar{r}^{1/4}) \right] \right\} - \bar{r}^{1/4} [1 - \bar{r}^{1/2}]^{3/2} \quad (28b)$$

The shape contours for the six body types listed above are compared in Figs. 5a and 5b for fineness ratios of 8 and 4 for laminar and turbulent flow, respectively. The laminar stable ablating nose tip shape in Fig. 5a most closely resembles the truncated sphere shape, whereas the turbulent stable shape in Fig. 5b is similar to the maximum heat transfer shape. The flat-nose height is smallest for the maximum heat transfer body, somewhat larger for the minimum drag body and largest for the minimum heat transfer body.

<sup>13</sup> Baker, R. L., "The Effect of Freestream and Material Parameters on Stable Ablating Nostip Shapes," Report No. TOR-0074(4450-76)-10, The Aerospace Corporation, El Segundo, California (May 1974).



The heat transfer integrals  $I_Q^L$  and  $I_Q^T$  are shown for these body shapes in Figs. 6a and 6b, respectively. The relative  $I_Q$  values for the different body shapes are generally similar for laminar and turbulent flow. The maximum solution  $I_Q$  values are up to four times greater than the minimum solution values with this ratio decreasing as  $\tau$  increases for  $2 < \tau < 8$ . This means that for this range of fineness ratio, the heat transfer for the laminar maximum solutions is up to two times greater than the laminar minimum solution values. The corresponding heat transfer increase for the minimum to maximum turbulent solutions is up to three times greater.

The  $I_Q$  values for truncated spheres, sharp cones, stable ablating shapes and minimum drag bodies all lie between the minimum and maximum solution values but tend to be much closer to the maximum value for a given  $\tau$ . An exception is the  $I_Q$  for minimum drag bodies for small  $\tau$ . The  $I_Q$  for these bodies peaks for  $\tau = 2$  and decreases for all other fineness ratios. At  $\tau = 2$ , the minimum drag body  $I_Q$ 's for laminar and turbulent flow are close to the corresponding maximum heat transfer solution values. However, for  $\tau$  decreasing and approaching zero ( $\tau < 0.02$ ), the minimum drag body  $I_Q$  values approach the minimum heat transfer body values. Maximum heat transfer solutions could not be found for  $\tau < 2$ .

### C. SOLUTION CHARACTERISTICS AND ACCURACY

Since many of the extremal solution body shapes discussed here have a flat nose followed by a body contour, it is of interest to compare these solutions in terms of the body angle immediately aft of the flat face and the ratio of flat-face height to base radius. For minimum heat transfer, minimum drag and maximum heat transfer bodies, the body angle aft of the flat face is about 4, 45, and 63 deg, respectively, independent of  $\tau$  and essentially independent of the boundary layer state, i.e., laminar or turbulent. This is shown in Table 1. Caution must be exercised concerning the maximum solutions. While the local flow at the expansion aft of the flat face is indicated to be supersonic using the present approximations, more exact calculations could

indicate subsonic flow at this location. The present formulation assumes the flow to be supersonic at the expansion corner. If this condition is not met, the proof of the existence of maximum solutions becomes much more difficult and the present solutions are not valid.

Table 1. Body Angle Aft of Expansion Corner for Different Variational Calculus Solutions

	<u>Laminar</u>	<u>Turbulent</u>
Minimum Heat Transfer Solution	3° 41'	3° 24'
Minimum Drag Solution	45°	45°
Maximum Heat Transfer	65° 39'	66° 23'

The flat face-base radius ratio for minimum heat transfer, maximum heat transfer and minimum drag shapes is shown in Fig. 7 as a function of fineness ratio. This ratio increases from essentially zero to 0.6-0.7, for  $\tau$  increasing from 2 to 10 for the maximum heat transfer solutions. For the minimum drag body, the flat-face height increases over the same range for fineness ratios from 0.2 to 10, and for the minimum heat transfer body the  $\tau$  range is about 0.02 to 10 for the same increase in flat-face height.

A final word of caution is in order regarding the accuracy of the predicted reduction in heat transfer associated with the minimum heat transfer shapes. Calculations using numerical inviscid flowfield computer codes for flat-face cones were carried out recently by Baker and Kramer<sup>10</sup>. These calculations indicate that while the local flow along the surface is highly over-expanded immediately aft of the flat-face expansion corner, the flow rapidly recompresses to pressure levels considerably above those for the same station on a sphere-cone. Because of this behavior, the reduction in heat transfer attributable to minimum heat transfer type shapes, when calculated using numerical flowfield calculation methods, is expected to be a factor of up to 2 rather than the factor of 3 predicted by the present work.

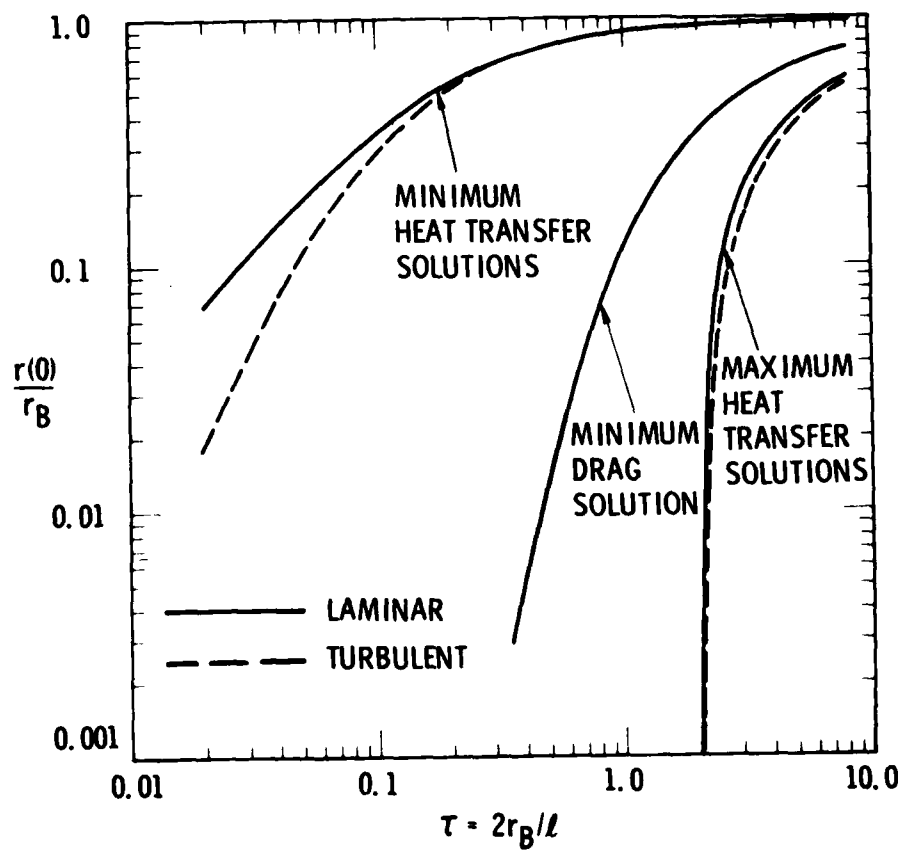


Fig. 7. Flat-Face Height versus Fineness Ratio

## V. SUMMARY AND CONCLUSIONS

Analytic expressions for total integrated heat transfer to a nose tip through a trajectory and variational calculus procedures have been used to determine nose tip shape contours having minimum total heat transfer for specified fineness ratio. Solutions for both laminar and turbulent boundary layer flow were obtained by numerical solution of the appropriate Euler equation and boundary conditions.

For fineness ratio  $\tau$  greater than zero, all solutions found have a flat face. The ratio of flat-face height to the base radius increases as  $\tau$  increases. As  $\tau$  becomes large ( $\tau > 10$ ), both the laminar and turbulent solutions approach a flat-faced cylinder of vanishing length, i.e., a disk. As  $\tau$  approaches zero ( $\tau < 0.02$ ), the solutions approach the slender body ( $\tau = 0$ ) solutions which are a  $1/2$  power law body for laminar flow and an  $8/13$  power law body for turbulent flow. For a constant base radius, the relative heat transfer rates to a family of minimum heat transfer shapes decreases monotonically as  $\tau$  decreases, i.e., as the bodies become more slender. For  $\tau \geq 0.02$ , the laminar and turbulent shapes are surprisingly similar to one another, i.e., the flat-face height to base radius ratio and the afterbody shape contour are essentially independent of the boundary layer state.

Additional solutions to the Euler equation depicting maximum heat transfer body shapes were found for  $\tau \geq 2$ . The heat transfer to the maximum solution shapes is up to two times greater than for the minimum solution shapes for laminar flow and up to three times greater for turbulent flow for  $2 < \tau < 8$ . Laminar and turbulent heat transfer rates to sharp cones, spheres, truncated spheres and stable ablating shapes were found to be generally much closer to the maximum solution values than to the minimum solution values. The laminar and turbulent heat transfer to a minimum drag body was also calculated.

The minimum and maximum solutions obtained could be shown mathematically to be minima and maxima only over restricted classes of body shapes. However, of all the physically reasonable additional body shapes considered, none were found which result in heat transfer rates lower than the minimum solution or greater than the maximum solution values.

# APPENDIX A

## SLENDER BODY MINIMUM HEAT TRANSFER SHAPES

Following the methods and nomenclature of Ref. 1, define the following nondimensional coordinates:

$$\eta = y, \quad \xi = \frac{\tau}{2} x$$

$$\tau = \frac{2R_B}{l} \quad (A-1)$$

Then, after differentiation and direct substitution into Eq. (17), we have

$$I_Q = \int_0^{2/\tau} \frac{y^{n+1} \dot{y}^2}{1 + \dot{y}^2} dx = \frac{\tau}{2} \int_0^1 \frac{\eta^{n+1} \eta^2}{1 + \left(\frac{\tau}{2}\right)^2 \dot{\eta}^2} d\xi, \quad \dot{\eta} = \frac{d\eta}{d\xi} \quad (A-2)$$

Since  $\tau^2 \ll 1$  for a slender body, in the slender body approximation the expression for  $I_Q$  becomes

$$(\text{Slender Body}) I_Q = \frac{\tau}{2} \int_0^1 \eta^{n+1} \eta^2 d\xi = \int_0^1 F(\eta, \xi) d\xi \quad (A-3)$$

For the case in which the function  $F$  is not an explicit function of the independent variable,  $\xi$ , the first integral of the Euler equation can be written immediately as

$$F - \dot{\eta} \frac{\partial F}{\partial \dot{\eta}} = C \quad (A-4)$$

Performing the indicated differential and algebraic manipulations, the following first integral of the Euler equation for this problem is obtained from Eqs. (A-3) and (A-4) after rearrangement

$$\frac{d\eta}{d\xi} = C\eta^{-(n+1)/2} \quad (\text{A-5})$$

The boundary conditions for Eq. (A-5) are

$$\eta(0) = 0$$

$$\eta(1) = 1 \quad (\text{A-6})$$

Integrating Eq. (A-5) and applying the boundary conditions, we obtain for laminar flow ( $n=1$ )

$$\eta = \xi^{1/2} \quad (\text{A-7})$$

and for turbulent flow ( $n=1/4$ )

$$\eta = \xi^{8/13} \quad (\text{A-8})$$

## APPENDIX B

### HEAT TRANSFER INTEGRALS--SLENDER BODY THEORY

The values of the heat transfer integrals  $I_Q^L$  and  $I_Q^T$  both go to zero as the fineness ratio,  $\tau$ , goes to zero. However, from Eq. (A-3), we have

$$\frac{2I_Q}{\tau} = \int_0^1 \eta^{n+1} \left( \frac{d\eta}{d\xi} \right)^2 d\xi \quad (B-1)$$

For laminar flow this becomes

$$\frac{2I_Q^L}{\tau} = \int_0^1 \eta^2 \left( \frac{d\eta}{d\xi} \right)^2 d\xi \quad (B-2)$$

From Eq. (A-7), for laminar flow

$$\eta = \xi^{1/2}, \quad \frac{d\eta}{d\xi} = \frac{1}{2} \xi^{-1/2} \quad (B-3)$$

Substituting Eq. (B-3) into Eq. (B-2) and integrating, we have

$$\frac{2I_Q^L}{\tau} = \int_0^1 \left( \xi^{1/2} \right)^2 \left( \frac{1}{2\xi^{1/2}} \right)^2 d\xi$$

$$\frac{I_Q^L}{\tau} = \frac{1}{8} \quad (B-4)$$



Similarly, for turbulent flow Eq. (B-1) becomes

$$\frac{2I_Q^T}{\tau} = \int_0^1 \eta^{5/4} \left( \frac{d\eta}{d\xi} \right)^2 d\xi \quad (B-5)$$

From Eq. (A-8), for turbulent flow

$$\eta = \xi^{8/13}, \quad \frac{d\eta}{d\xi} = 8/13 \xi^{-5/13} \quad (B-6)$$

Substituting and integrating, we have

$$\frac{2I_Q^T}{\tau} = \int_0^1 \left( \xi^{8/13} \right)^{5/4} \left( 8/13 \xi^{-5/13} \right)^2 d\xi$$

$$\frac{I_Q^T}{\tau} = \frac{32}{169} \quad (B-7)$$

Comparing the numerical values of  $I_Q^L$  and  $I_Q^T$  from Eqs. (B-4) and (B-7) with the non-slender body calculated values in Fig. 5, we see that for  $\tau < 0.02$  the slender and non-slender body calculated values are very close to one another.

# APPENDIX C

## STABLE ABLATING NOSETIP SHAPES

The transient shape change equation derived in Ref. 10 becomes after differentiation with respect to  $s$  and appropriate substitutions related to the geometry of Fig. 1

$$\left(\frac{\partial \alpha}{\partial t}\right)_s = \frac{1}{\sin \alpha} \frac{\partial}{\partial s} \left[ \frac{\dot{q}}{Q^* \sin \alpha} \right] \quad (C-1)$$

For a steady-state condition, i.e., a stable ablating nosetip shape, the local body angle,  $\alpha$ , is not a function of time. Thus

$$\frac{d}{ds} \left[ \frac{\dot{q}}{Q^* \sin \alpha} \right] = 0 \quad (C-2)$$

Integrating

$$\frac{\dot{q}}{Q^* \sin \alpha} = \text{constant} = C_1 \quad (C-3)$$

We wish to determine the body shape such that the heat transfer distribution  $\dot{q} = \dot{q}(\alpha, s)$  will satisfy Eq. (C-3). From Ref. 10, for laminar flow in the boundary layer

$$\dot{q}^L = \frac{C^L \rho_e u_e \mu_e r}{\left[ 2 \int_0^s \rho_e u_e \mu_e r^2 ds \right]^{1/2}} \quad (C-4)$$

Combining Eqs. (C-3) and (C-4) and assuming that the effective heat of ablation,  $Q^*$ , is constant

$$\frac{\dot{q}L}{\sin\alpha} = C_1 Q^* = \frac{C^L \left( \frac{\rho_e u_e \mu_e r}{\sin\alpha} \right)}{\left[ 2 \int_0^r \frac{\rho_e u_e \mu_e r^2 dr}{\sin\alpha} \right]^{1/2}} \quad (C-5)$$

Let

$$f = \frac{\rho_e u_e \mu_e}{\sin\alpha} \quad (C-6)$$

Then Eq. (C-5) becomes

$$\frac{\dot{q}}{\sin\alpha} = C_1 Q^* = \frac{C^L f r}{\left[ 2 \int_0^r f r^2 dr \right]^{1/2}} \quad (C-7)$$

By direct substitution, we find that Eq. (C-7) is satisfied by

$$f = \frac{1}{2} \left[ \frac{C_1 Q^*}{C^L} \right]^2 r \quad (C-8)$$

Combining Eqs. (C-6) and (C-8) together with Eqs. (11) through (13) and the trigonometric relations

$$\dot{r} = \frac{dr}{dz} = \tan\alpha, \quad \sin\alpha = \frac{\dot{r}}{\sqrt{1 + \dot{r}^2}}, \quad \cos\alpha = \frac{1}{\sqrt{1 + \dot{r}^2}} \quad (C-9)$$

the following differential equation for the laminar stable ablating nosetip shape is obtained;

$$\dot{r} = \frac{2A^L - \sqrt{4(A^L)^2 - 4r^2}}{2r} \quad (C-10)$$

where  $A^L = (C_1 Q^* / C^L)^2$ , or defining  $\bar{r} = r / A^L$

$$\frac{\dot{z}}{r^2} = \frac{1 - \sqrt{1 - \bar{r}^2}}{\bar{r}} \quad (C-10b)$$

Integrating Eq. (C-10) and applying the boundary condition  $z(0) = 0$ , we obtain

$$\bar{z} = \frac{z}{A^L} = \ln \left[ \frac{1 + \sqrt{1 - \bar{r}^2}}{2} \right] - \sqrt{1 - \bar{r}^2} + 1 \quad (C-11)$$

For turbulent flow in the boundary layer we have from Ref. 11

$$\dot{q}^T = \frac{C^T \rho_e^u \mu_e r^{1/4}}{\left[ \int_0^s \rho_e^u \mu_e r^{5/4} ds \right]^{1/5}} \quad (C-12)$$

Applying the same procedures as in the laminar case above, we find that the differential equation describing the turbulent stable ablating shape is

$$\dot{r} = \frac{2A_T \sqrt{4(A_T)^2 - 4r^{1/2}}}{2r^{1/4}}$$

$$A_T = \frac{1}{2} \left( \frac{5}{2} \right)^{1/2} \left( \frac{C_1 Q^*}{C^T} \right)^{-5/4} \quad (C-13)$$

Integrating Eq. (C-13) with the aid of the substitution  $X = r^{1/4}$ , applying the boundary condition  $z(0) = 0$  and nondimensionalizing, we obtain

$$\bar{z} = \frac{z}{A_T} = \frac{4}{3} \bar{r}^{3/4} - \left[ \frac{1}{2} \left\{ \bar{r}^{1/4} \sqrt{1 - \bar{r}^{1/2}} + \sin^{-1} \bar{r}^{1/4} \right\} \right] - \bar{r}^{1/4} \left[ 1 - \bar{r}^{1/2} \right]^{3/2} \quad (C-14)$$